Chinese Chemical Letters 36 (2025) 110098

Contents lists available at ScienceDirect

Chinese Chemical Letters

journal homepage: www.elsevier.com/locate/cclet

NIR-II emissive aza-BODIPY-based nanoparticles for triggering glioblastoma apoptosis in brain

Mengjie Gao[a,1], Zhiqiang Cui[b,d,1], Yue Shen[a], Yikun Li[c], Dongxiang Zhang[a], Xiaoyan Gao[b,e], Yaguang Sun[f], Xin-Dong Jiang[a,*], Jianjun Du[c,*], Xiaohong Sun[b,e,*]

[a] Liaoning & Shenyang Key Laboratory of Functional Dye and Pigment, Shenyang University of Chemical Technology, Shenyang 110142, China
[b] Department of Neurology, The Fourth Affiliated Hospital of China Medical University, Shenyang 110032, China
[c] State Key Laboratory of Fine Chemicals, Dalian University of Technology, Dalian 116024, China
[d] Department of Ion Channel Pharmacology, School of Pharmacy, China Medical University, Shenyang 110032, China
[e] Science Experiment Center, China Medical University, Shenyang 110032, China
[f] Key Laboratory of Inorganic Molecule-Based Chemistry of Liaoning Province, Shenyang University of Chemical Technology, Shenyang 110142, China

ARTICLE INFO

Article history:
Received 7 April 2024
Revised 3 June 2024
Accepted 5 June 2024
Available online 6 June 2024

Keywords:
Glioblastoma
NIR-II
aza-BODIPY
PTT
Apoptosis

ABSTRACT

D-D'-A type aza-borondipyrromethenes (aza-BODIPYs) were prepared by Suzuki cross-coupling reaction. Photothermal conversion efficiency of self-assemble aza-BODIPY-based nanoparticles (DA-azaBDP-NPs) with NIR-II emission ($\lambda_{em} = 1065$ nm) was 37.2% under near infrared (NIR) irradiation, and the outstanding cytotoxicity was triggered by coexistence of DA-azaBDP-NPs and the NIR irradiation, with the decrease of glioblastoma migration and the inhibition of glioblastoma proliferation. DA-azaBDP-NPs could promote glioblastoma autophagy and accelerate the process of cell death. The photothermal therapy (PTT) of DA-azaBDP-NPs can effectively induce glioblastoma death by apoptosis under the NIR irradiation, which is highly promising to be applied *in vivo* experiments of brain.

Glioblastoma (GBM) is one of the most common primary tumor in the central nervous system, which is characterized by high malignancy, strong invasion and poor prognosis [1,2]. Tumor resection assisted postoperative radiotherapy and chemotherapy is the current mainstream therapy of glioblastoma patients [3]. The clinical doctors have been bothered by the situation that GBM is difficult to be resected completely with poor sensitiveness to chemotherapy drugs [4,5]. In addition, most drug molecules are unable to fully penetrate into the intracranial focus and exert therapeutic effects because of the existence of blood-brain barrier [6]. Therefore, it is urgent that the occurrence of new technology or new targeted drugs facilitates the clinical treatment of glioblastoma. Very recently, the great potential of optically active dye nanoparticles with near-infrared active-targeting photothermal therapy (PTT) for the treatment of brain tumors, has been attracting increasing interest [7,8].

Near infrared (NIR) dyes with strong absorption in NIR-I window (NIR-I, 700–900 nm) can reduce the absorption and scattering of light by tissues, as well as the self-fluorescence of tissues, resulting in a significant increase in imaging depth [7,9]. However, it still cannot meet the needs of clinical applications for deep tissues [10,11]. NIR II (900–1700 nm) fluorescence imaging is a low scattering, deep tissue and organ penetration, and high-resolution imaging [12-16]. *In vivo* imaging technology with resolution and no risk of ionizing radiation has received widespread attention in the field of tumor diagnosis and treatment [17-21]. Due to the advantages of deep tissue penetration depth and high spatiotemporal resolution, fluorescence imaging technology in NIR-II region has rapidly developed, and its potential application in clinical diagnosis and treatment of tumors has been attracted increasing attention. Especially, PTT has been regarded as an alternative way of curing cancer [22-24]. PTT converts light energy into heat by photothermal agents (PTAs) to increase the temperature of the surrounding microenvironment, resulting in localized thermal damage and eliminating cancer cells [25-31]. Owing to the outstanding behavior, functional organic dyes are currently serving as an appropriate platform for PTAs.

Among traditional functional organic dyes [32,33], aza-BODIPY has attracted increasing interest, due to its long wavelength, high molar extinction coefficient and modifiability [34,35]. Recently, aza-BODIPY platform has shown unique applications in

* Corresponding authors.
E-mail addresses: xdjiang@syuct.edu.cn (X.-D. Jiang), dujj@dlut.edu.cn (J. Du), xhsun@cmu.edu.cn (X. Sun).
[1] These authors contributed equally to this work.

https://doi.org/10.1016/j.cclet.2024.110098
1001-8417/

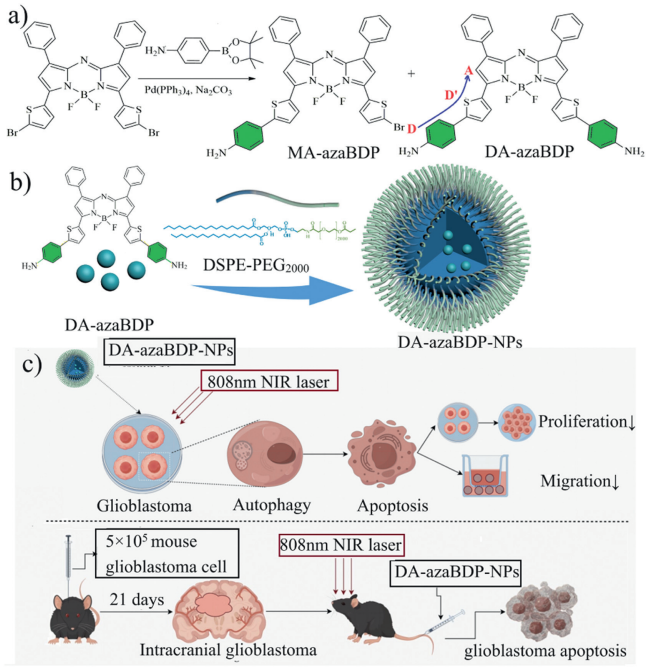

Scheme 1. (a) Synthesis of D-D'-A type aza-BODIPYs MA-azaBDP and DA-azaBDP. (b) Self-assembly of DA-azaBDP-NPs. (c) Schematic diagram about effect of DA-azaBDP-NPs under laser irradiation on the GBM cells.

biomedical applications [36,37]. However, there are few reported cases in which the absorption or emission maxima of aza-BODIPY have touched the NIR-II region [38]. Herein, thiophene-substituted aza-BODIPY nucleus platform ($\lambda_{em} = 751$ nm) was wisely chosen to prepare D-D'-A type molecules by electron donating groups (Scheme 1a) [39], reaching the NIR-II region (DA-azaBDP-NPs: $\lambda_{em} = 1065$ nm) (Scheme 1b) [40,41]. To enhance the water solubility and biocompatibility for photoimaging and phototherapy in biological system, self-assembled dye nanoparticles DA-azaBDP-NPs were employed to explore photothermal therapy. Remarkable cytotoxicity was triggered by coexistence of NIR-II DA-azaBDP-NPs and the NIR irradiation, with the decrease of GBM cell migration and the inhibition of GBM cell proliferation (Scheme 1c). DA-azaBDP-NPs could promote GBM cell autophagy and accelerate the process of cell death. The PTT of DA-azaBDP-NPs can effectively induce GBM cell death by apoptosis under NIR irradiation. *In vivo* experiments of brain were estimated for the good tumor-inhibition capability with promoting the apoptosis and autophagy level of glioblastoma cells by the DA-azaBDP-NPs under the NIR irradiation (Scheme 1c).

To construct aza-BODIPY dye with NIR-II emission, Suzuki cross-coupling strategy was employed [42,43]. NIR-I absorbing aza-BODIPY as a raw material was ingeniously chosen to couple with (4-aminophenyl)boronic acid, introducing strong electron donating group (Scheme 1a) [44]. Monoaniline substituted aza-BODIPY (MA-azaBDP) and dianiline substituted aza-BODIPY (DA-azaBDP) were successfully prepared, respectively. Next, we first gain insight into the spectral performance of the new aza-BODIPYs. The absorption maximum of MA-azaBDP is 784 nm and bathochromic-shifted by 47 nm (Fig. 1a), comparing to that of the parent dye aza-BODIPY ($\lambda_{abs} = 727$ nm in CH_2Cl_2) [44]. Especially, DA-azaBDP absorbs at 838 nm (Fig. 1a), along with high molar extinction coefficient (ε = 195,000 L mol^{-1} cm^{-1}) and full width half maximum (FWHM = 106 nm). Moreover, the highest occupied molecular orbital (HOMO) is localized largely on the core including aniline segment in DA-azaBDP, while the lowest unoccupied molecular orbital (LUMO) mainly lies on the core including 1,7-phenyl groups (Inner panel of Fig. 1a). Such a large separation of HOMO and LUMO distributions is a typical characteristic of charge-transfer (CT) molecule for DA-azaBDP, in which the push-pull effect (D-D'-A) is remarkable (Fig. 1a, Scheme 1a). And, quantum-chemical study between DA-azaBDP (LUMO/HOMO (eV) = 1.70) and MA-azaBDP (LUMO/HOMO (eV) = 1.82) well explained and supported the difference of their absorption (Fig. S1 in Supporting information).

Using the amphiphilic co-polymer 1,2-distearoyl-*sn*–glycero-3-phosphoethanolamine-*N*-[hydroxyl(poly(ethyleneglycol))–2000] (DSPE-PEG_{2000}) as the encapsulating medium [45,46], dye-nanoparticles MA-azaBDP-NPs and DA-azaBDP-NPs by self-assembly were obtained, respectively (Figs. 1b–f, Fig. S2 in Supporting information). The hydrophobic segment aggregated in the core, whereas the hydrophilic PEG_{2000} chain constructed the shell, providing water-soluble DA-azaBDP-NPs (Scheme 1b). DA-azaBDP-NPs showed spherical morphology (Fig. 1f), based on the transmission electron microscopy (TEM) photographs. Dynamic light scattering (DLS) of DA-azaBDP-NPs indicated that the dye NPs hydrodynamic diameters was 137 nm and the polymer dispersity index (PDI) is 0.359 (Fig. 1e). Owing to the π-π stacking in the encapsulated dye polymer, the absorption maximum of DA-azaBDP-NPs in aqueous solution was bathochromic-shifted to 876 nm and the absorption band became wider, covering from 700 nm to 1000 nm (Fig. 1b), comparing to that (838 nm) of DA-azaBDP in CH_2Cl_2 (Fig. 1a). The emission maximum of the DA-azaBDP-NPs is 923 and 1065 nm in the NIR-II region (Figs. 1g and h). Additionally, for MA-azaBDP-NPs, the absorption maximum in aqueous solution was 808 nm (Fig. 1b, Table S1 in Supporting information).

Based on Jablonski Diagram [47-49], a relaxed molecule in the lowest vibrational level of the excited state is well-known to return to the ground state mainly *via* the radiative transition (fluorescence), the non-radiative transition (heat release) and intersystem crossing (ISC) to the triplet, sensitizing oxygen to produce reactive oxygen species (ROS) [50,51]. Due to the low fluorescence quantum yield (Table S1) and low singlet oxygen generation efficiency (Fig. S3 in Supporting information) of these dyes, we will explore their photothermal conversion (Figs. 1i–n, Figs. S4 and S5 in Supporting information). The temperature increased remarkably by 915 nm laser irradiation (0.8 W/cm^2) of DA-azaBDP-NPs in the aqueous solution (Fig. 1i). When 5 min light irradiation, the solution temperature even reached 57.4 °C from 28.5 °C (Fig. 1i), achieving strong light absorption ability and thermal energy release properties. The temperature enhancement at different concentrations of DA-azaBDP-NPs and different optical power densities were measured. According to Figs. 1j and k, temperature promotion is dependent on concentration and power density. Higher concentration and stronger power density resulted in better thermal conversion. In Fig. 1l, the solution temperature in the heating phase achieved a rapid heating effect for 5 min. Once stopping the radiation, the temperature of the solution cooled rapidly to near room temperature after 5 min, and the cooling effect was not significant for the next 5 min. Based on Fig. 1l, the temperature changes during the heating-cooling cycle of each group are almost the same, indicating that DA-azaBDP-NPs had the outstanding photothermal stability and can be applied for photothermal therapy for multiple cycles. Moreover, the associated time constant obtained by mapping the cooling time and driving force temperature was brought into the reported formula for calculating the photothermal conversion efficiency (PEC) (Figs. 1m and n). The PEC of DA-azaBDP-NPs was calculated to be 37.2%, which is great in agreement with that of the previously reported reputable PTAs [52,53]. Additionally, the PEC of DA-azaBDP-NPs with 808 nm laser irradiation was calculated to be 34.6% (Fig. S5).

By using the cell counting kit-8 (CCK-8) assay, the phototoxicity of DA-azaBDP-NPs to U251, LN229 and U87-MG glioblastoma cells was investigated. Without irradiation, the three glioblas-

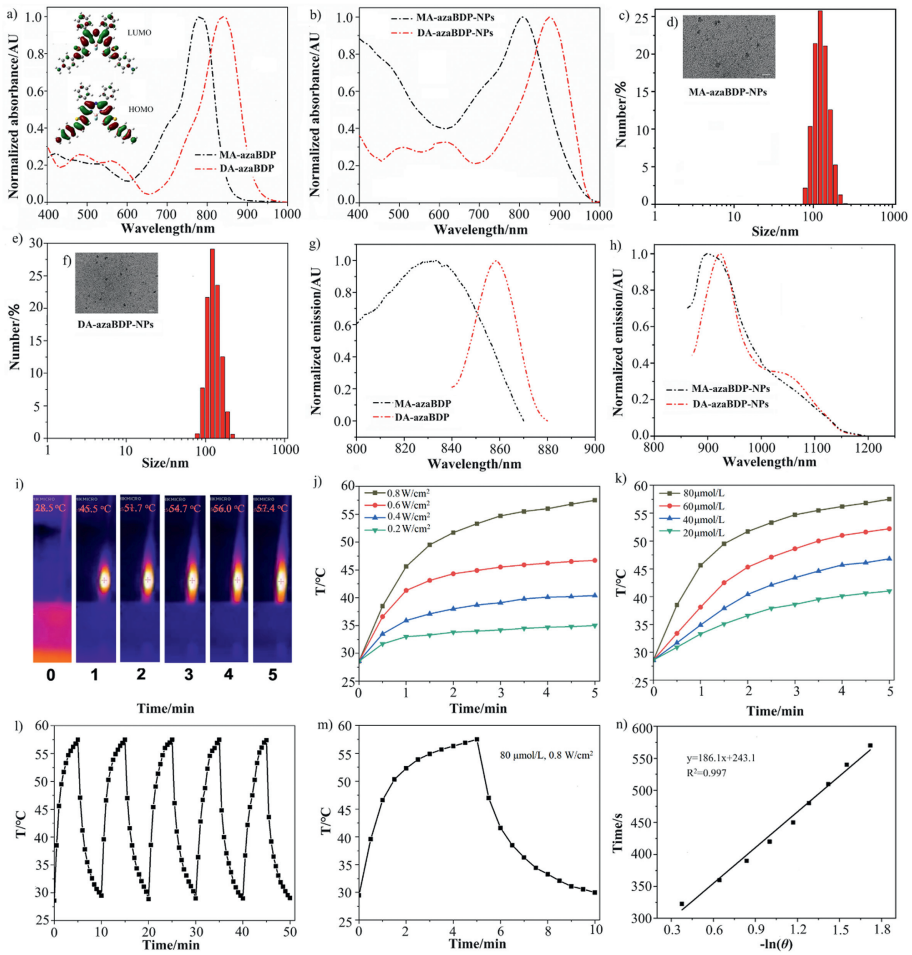

Fig. 1. (a) Normalized absorption spectra of MA-azaBDP (black curve) and DA-azaBDP (red curve) in CH_2Cl_2. Inner panel displayed frontier molecular orbitals of DA-azaBDP at the B3LYP/6–31G(d) level with Gaussian 09. LUMO/HOMO (eV) = −2.92/−4.62. (b) Normalized absorption spectra of MA-azaBDP-NPs (black curve) and DA-azaBDP-NPs (red curve) in aqueous solution. (c) DLS and (d) TEM of MA-azaBDP-NPs in aqueous solution. (e) DLS and (f) TEM of DA-azaBDP-NPs in aqueous solution. Scale bar: 200 nm. (g) Normalized emission spectra of MA-azaBDP (black curve) and DA-azaBDP (red curve) in CH_2Cl_2 at 298 K. (h) Normalized emission spectra of MA-azaBDP-NPs (black curve) and DA-azaBDP-NPs (red curve) in aqueous solution at 298 K. (i) Photothermal imaging of DA-azaBDP NPs in aqueous solution (80 μmol/L) at different temperature before or after 915 nm laser (0.8 W/cm^2) irradiation. (j) Photothermal conversion of DA-azaBDP NPs (80 μmol/L) under 915 nm laser irradiation with different power density (0.2, 0.4, 0.6 and 0.8 W/cm^2). (k) Photothermal conversion of DA-azaBDP NPs at different concentrations (20, 40, 60 and 80 μmol/L) under laser irradiation (0.8 W/cm^2). (l) Photothermal stability study during five circles of heating-cooling processes. (m) Photothermal effect of DA-azaBDP NPs in aqueous solution irradiated by 915 nm laser (0.8 W/cm^2) for 5 min and then irradiation. (n) Plot of cooling time of DA-azaBDP NPs *versus* negative natural logarithm of the temperature from the cooling test.

toma cell lines were tested for dose-dependent cytotoxicity of DA-azaBDP-NPs (Figs. 2a–c). Even at high concentrations, the cytotoxicity was barely observed, indicating the strong biocompatibility of DA-azaBDP-NPs. However, when exposed to a 0.3 W/cm^2 (808 nm) laser for 10 min, there was a noticeable drop in cell viability with the increasing concentration of DA-azaBDP-NPs. The findings showed that low intensity NIR irradiation may cause the photothermal effect of DA-azaBDP-NPs in cells, leading to kill glioblastoma cells effectively. To visualize the effectiveness of phototherapeutic capacity of DA-azaBDP-NPs, live-dead cell staining was performed by double-staining calcein AM (green) and propidium iodide (PI, red) dyes. Green fluorescence represents the live cells and red indicates the dead ones. As expected, DA-azaBDP-NPs induced complete destruction of LN229 cells after NIR laser irradiation (0.3 W/cm^2, 10 min) as shown by the red fluorescence. However, only green fluorescence, the indicator of live cells, was observed in the sole light or sole DA-azaBDP-NPs groups, suggesting that remarkable cytotoxicity was triggered by coexistence of the DA-azaBDP-NPs and NIR irradiation (Fig. 2d). Cell migration and proliferation is a characteristic of tumors and is closely related to the degree of malignancy of the tumor [54-56]. To evaluate the ability of cell migration, the transwell assay was used (Fig. 2e). The result of transwell assay demonstrated that the proportion of crystal violet dye solution stained cells in Group NPs+Light was smaller than Group Light or Group NPs, which reflected a significant decrease of cell migration rate with incubation of DA-azaBDP-NPs under NIR irradiation. Furthermore, the cells in proliferation were stained with EdU (green), while nucleus stained with 4,6-diamino-2-phenyl indole (DAPI) (blue) (Fig. 2f). Edu, belonging to the thymidine nucleoside analogue, was regarded as the indicator of cell proliferation. In Group NPs+Light, the green fluorescence from EdU-stained cells was merely observed, while the images from the other three groups showing the green fluorescence obviously, which suggested that the proliferative ability of cells stimulated by the NIR irradiation or DA-azaBDP-NPs incubation only was undamaged. The influence of DA-azaBDP-NPs about inhibiting cell proliferation on glioblastoma cells was able to work under the circumstance of the existence of NIR irradiation.

Recently, autophagy is found to play an important regulatory role in the biogenesis and development of various tumors. Autophagy is a normal physiological process of cells, closely related to the biogenesis and development of tumors. The level of autophagy plays a key role in the proliferation and migration ability of tumor cells [57-59]. To investigate the photothermal effect

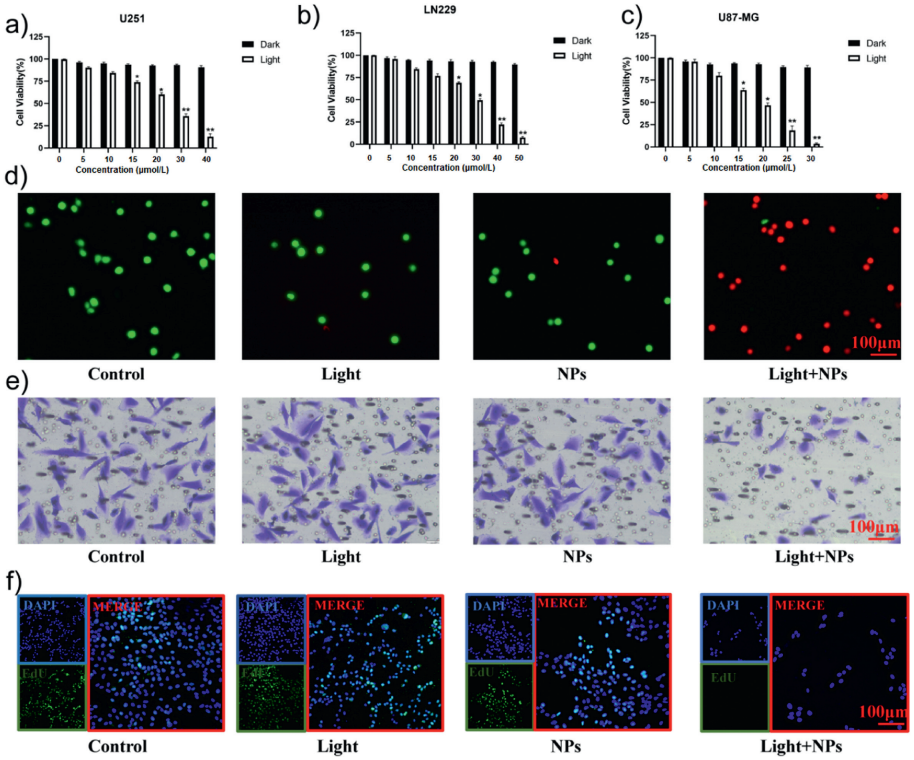

Fig. 2. Photothermal effect of DA-azaBDP-NPs under 808 nm laser irradiation on the migration and proliferation ability of glioblastoma cell. (a–c) Cell viability was analyzed by CCK-8 assay in three glioblastoma cell lines (U251, LN229 and U87-MG) under different concentrations with 808 nm laser irradiation. (d) Fluorescence images of calcein AM and PI co-stained LN229 cells. (e) Representative images of transwell assay were used to evaluate the ability of cell migration. (f) Representative images of EdU staining were used to evaluate the ability of cellproliferation. Data are presented as mean ± standard deviation (SD) ($n = 3$). $^{*}P < 0.05$, $^{**}P < 0.01$ *vs.* Group 0 μmol/L. Scale bar: 100 μm. Group Control: untreated glioblastoma cell LN229; Group Light: glioblastoma cellLN229 under 808 nm laser irradiation (0.3 W/cm^2) for 10 min without incubation of DA-azaBDP-NPs; Group NPs: glioblastoma cell LN229 incubated by 30 μmol/L DA-azaBDP-NPs without laser irradiation (0.3 W/cm^2) for 10 min; Group NPs+Light: glioblastoma cell LN229 incubated by 30 μmol/L DA-azaBDP-NPs under laser irradiation (0.3 W/cm^2) for 10 min. 30 μmol/L DA-azaBDP-NPs were abbreviated as NPs in Fig. 2.

of DA-azaBDP-NPs mediated glioblastoma cell death, we first start with autophagy as the entry point. Firstly, we observed the expression levels of autophagy related biomarkers in each group of cells (Figs. 3a–c). The Western blot results showed the expression level of Beclin1 and the ratio of MAP1LC3 (LC3)-II/LC3-I in Group NPs+Light were higher than the other three groups, while the expression level of p62 reduced correspondingly. Electron microscopy, as a commonly used measurement in cell autophagy researches, can be used for observing the ultrastructure of cells more directly, reflecting typical autophagic manifestations such as changes in mitochondrial structure and secretion of autophagic vesicles [60,61]. From the electron microscopy results, the mitochondrial structural damage and the secretion of more autophagic vesicles were shown in Group NPs+Light (Fig. 3d). The above-mentioned results indicate that DA-azaBDP-NPs could promote cell autophagy and accelerate the process of cell death (Fig. 3d).

We further studied the role of cell apoptosis under hyperthermia induced by DA-azaBDP-NPs. Firstly, we observed the expression levels of apoptosis related biomarkers in each group of cells. The Western blot results showed the expression level of BAX and cleaved-caspase 3 in Group NPs+Light were higher than the other three groups, while the expression level of BCL2 decreased accordingly (Figs. 4a and b). Flow cytometry assay was performed to quantify the apoptosis level of glioblastoma cell. The apoptosis cells were stained with Annexin-V (green), while necroptosis cells stained with PI (red). The second and fourth quadrants represent cells during the late and early apoptosis period, respectively [62,63]. The percentage of apoptosis cells increased from 18.8% (blank control) to 51.8% after treatment with 0.3 W/cm^2 from an 808 nm NIR laser for 10 min (Fig. 4c), further confirming the efficient apoptosis-inducing capacity of DA-azaBDP-NPs to glioblastoma cells. The production of reactive oxygen species (ROS) was usually accompanied with the occurrence of apoptosis [64]. To explore whether DA-azaBDP-NPs combined with 808 nm NIR laser

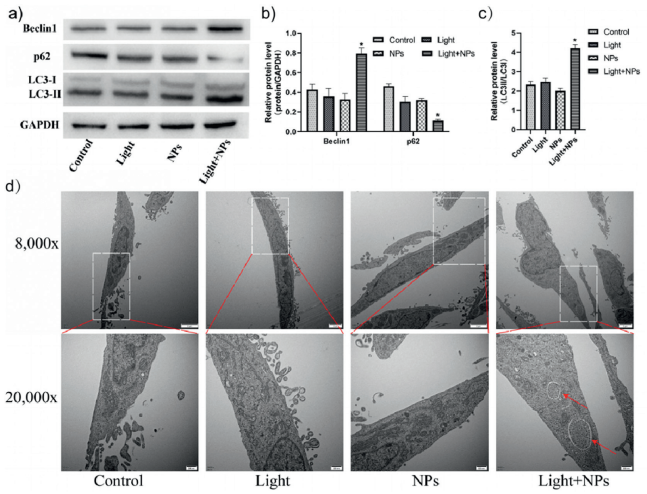

Fig. 3. Effect of DA-azaBDP-NPs under 808 nm laser irradiation (0.3 W/cm^2) on the autophagy process of glioblastoma cell. (a–c) Protein expression levels of autophagy-related indicators (Beclin 1, p62, LC3I, LC3II) were evaluated by Western blot (a). Quantification analysis of expression of Beclin 1, p62, LC3-I, LC3-II (b, c). (d) Representative transmisssion electron microscopy images of glioblastoma cell LN229 (magnification 8000× and 20,000×, respectively). Scale bar: 2 μm for 8000×; 500 nm for 20,000×. Data are presented as mean ± SD ($n = 3$). $^{*}P < 0.05$, $^{**}P < 0.01$ *vs.* Group Control. 30 μmol/L DA-azaBDP-NPs were abbreviated as NPs in Fig. 3. GAPDH, glyceraldehyde-3-phosphate dehydrogenase.

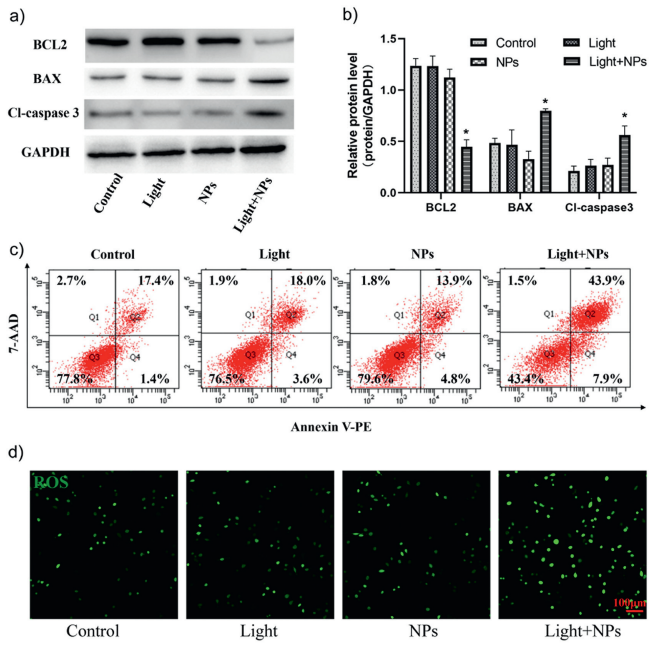

Fig. 4. Effect of DA-azaBDP-NPs under 808 nm laser irradiation (0.3 W/cm^2) on the apoptosis of glioblastoma cells. (a) Protein expression levels of apoptosis-related indicators (B-cell lymphoma-2 (BCL2), BCL2-associated X (BAX) and cleaved-caspase 3 (Cl-caspase 3)) were evaluated by Western blot. (b) Quantification analysis of expression of BCL2, BAX and Cl-caspase 3. (c) Flow cytometry assay was used to quantify the apoptosis levels of glioblastoma cell LN229. (d) Representative images of intracellular ROS level from four groups of glioblastoma cell LN229. Scale bar: 100 μm. Data are presented as mean ± SD ($n = 3$). $^*P < 0.05$, $^{**}P < 0.01$ *vs.* Group Control. 30 μmol/L DA-azaBDP-NPs were abbreviated as NPs in Fig. 4.

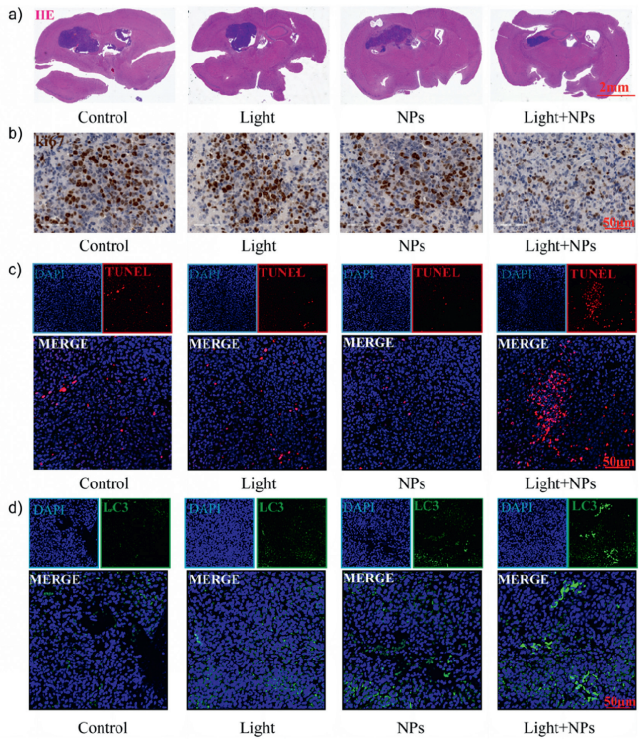

Fig. 5. (a) HE stained images of the intracranial tumor area after different treatments (5×). Scale bar: 2 mm. (b) Immunohistochemical Ki67 (proliferation marker) stained images of the intracranial tumor from four groups (400×). Scale bar: 50 μm. (c) TUNEL (apoptosis marker) stained images of the intracranial tumor area after different treatments (400×). Scale bar: 50 μm. (d) Immunohistochemical LC3 (autophagy marker) stained images of the intracranial tumor from four groups (400×). Scale bar: 50 μm.

would influence the production of ROS from glioblastoma, we used the ROS probe DCFH-DA to indicate the ROS level from each group. Under green light excitation, the fluorescence intensity from Group NPs+Light was higher than the other three groups (Fig. 4d). Combined with the above results, DA-azaBDP-NPs can effectively induce tumor cell death under NIR irradiation with low intensity.

In view of the inspiriting results from the above experiments about glioblastoma cells, *in vivo* experiments with 6 mice in each group were conducted to further evaluate the apoptosis-inducing effect of DA-azaBDP-NPs combined with 808 nm NIR laser (Fig. 5). All animal experiments were approved by the Animal Experimental Ethics Committee of China medical university. Firstly, the mice were injected with a dose of 5×10^5 GL261 mouse glioblastoma cells intracerebrally by a stereotaxic technique [65]. After 21 days, they were randomly grouped into four groups, and each group was received with different treatments, as follows: mice without treatment (group Control); mice with irradiation of 808 nm NIR laser (group Light); mice with the injection of DA-azaBDP-NPs *via* the tail vein (group NPs); mice with the combination of laser irradiation and DA-azaBDP-NPs injection (group Light+NPs). To evaluate the intracranial tumor size from four groups, HE staining was performed to assess overall morphology of mouse brains. The results from HE staining showed that compared with group Control, the tumor size in the sole light and sole NPs groups was no significant differences (Fig. 5a). However, the tumor size in the group Light+NPs decreased obviously compared the other three groups (Fig. 5a). Cellular proliferation and apoptosis may acted as the main characters during the tumor growth [66,67]. Ki67 was a cellular proliferation marker and positively correlated with the malignant degree of glioblastoma [68]. The proliferation of tumor cells can be examined by immunohistochemistry staining against Ki67. Immunohistochemistry results revealed the expression level of Ki67 in the area of intracranial tumors from group Light+NPs was lower than group Light or group NPs, suggesting the combination of laser irradiation and DA-azaBDP-NPs injection could inhibit the cellular proliferation of glioblastoma (Fig. 5b). In the other hand, the TdT-mediated dUTP nick-end labeling (TUNEL) staining was used to measure the apoptosis level of intracranial glioblastoma from each group [69]. The apoptotic cells were stained with TUNEL (Red), while nucleus stained with DAPI (blue). Similar to the *in vitro* result, the combination of laser irradiation and DA-azaBDP-NPs injection could promote the apoptosis of glioblastoma on the basis of red fluorescent expression (Fig. 5c). LC3 is the essential autophagy protein and represents the activity of autophagy [70]. In our immunofluorescence experiments, autophagic tumor cells were stained with LC3 (Green), while nucleus stained with DAPI (blue). Immunofluorescence assay demonstrated that the autophagic level of mouse glioblastoma cells from group Light+NPs was upregulated compared with the other three groups according to the fluorescent expression from LC3 (Fig. 5d). These results clearly confirmed the good tumor-inhibition capability with promoting the apoptosis and autophagy level of glioblastoma cells by the DA-azaBDP-NPs under NIR irradiation.

In summary, using Suzuki cross-coupling reaction, monoaniline substituted aza-BODIPY (MA-azaBDP) and dianiline substituted aza-BODIPY (DA-azaBDP) were synthesized by reaction of thiophene-substituted aza-BODIPY with (4-aminophenyl)boronic acid. Dye-nanoparticles MA-azaBDP-NPs and DA-azaBDP-NPs by self-assembly absorb at 808 and 876 nm respectively. Photothermal conversion efficiency of DA-azaBDP-NPs with NIR-II emission ($\lambda_{em} = 1065$ nm) was 37.2% under NIR irradiation, and the outstanding cytotoxicity was triggered by DA-azaBDP-NPs under the NIR irradiation, with the decrease of glioblastoma cell migration and the inhibition of glioblastoma cell proliferation. DA-azaBDP-

NPs could promote glioblastoma cell autophagy and accelerate the process of cell death. The PTT of DA-azaBDP-NPs can effectively induce glioblastoma cell death by apoptosis under the NIR irradiation, which is highly promising to be applied *in vivo* experiments of brain.

Declaration of competing interests

The authors declare that they have no known competing financial interests or personal relationships that could have appeared to influence the work reported in this paper.

CRediT authorship contribution statement

Mengjie Gao: Investigation, Data curation. **Zhiqiang Cui:** Software, Methodology. **Yue Shen:** Software. **Yikun Li:** Methodology. **Dongxiang Zhang:** Writing – original draft. **Xiaoyan Gao:** Resources, Methodology. **Yaguang Sun:** Investigation. **Xin-Dong Jiang:** Writing – review & editing, Resources. **Jianjun Du:** Writing – review & editing. **Xiaohong Sun:** Writing – review & editing.

Acknowledgments

This work was supported by the National Natural Science Foundation of China (Nos. 22078201, U1908202), Liaoning & Shenyang Key Laboratory of Functional Dye and Pigment (Nos. 2021JH13/10200018, 21–104–0-23).

Supplementary materials

Supplementary material associated with this article can be found, in the online version, at doi:10.1016/j.cclet.2024.110098.

References

[1] L.R. Schaff, I.K. Mellinghoff, JAMA 329 (2023) 574–587.
[2] T.S.V. Solinge, L. Nieland, E.A. Chiocca, et al., Nat. Rev. Neurol. 18 (2022) 221–236.
[3] E.L. Rhun, M. Preusser, P. Roth, et al., Cancer. Treat. Rev. 80 (2019) 101896.
[4] J.S. Castresana, B. Meléndez, Cells 12 (2023) 2063.
[5] A. Ou, W. Yung, N. Majd, Int. J. Mol. Sci. 22 (2020) 351.
[6] P.S. Steeg, Nat. Rev. Clin Oncol. 18 (2021) 696–714.
[7] Y. Jia, X. Wang, D. Hu, et al., ACS Nano 13 (2019) 386–398.
[8] I. Hasan, S. Roy, E. Ehexige, et al., Nanoscale 15 (2023) 18108–18138.
[9] J. Lin, B. Xing, D. Jin, Adv. Opt. Mater. 11 (2023) 2300802.
[10] Y. Jiang, J. Li, X. Zhen, et al., Adv. Mater. 30 (2018) e1705980.
[11] J. Cao, B. Zhu, K. Zheng, et al., Front. Bioeng. Biotechnol. 7 (2020) 487.
[12] B. Sun, K.S. Hettie, S. Zhu, Adv. Ther. 4 (2021) 2000278.
[13] Y. Wang, D. Zhang, K. Xiong, et al., Chin. Chem. Lett. 33 (2022) 115–122.
[14] H. Wang, X. Mu, J. Yang, et al., Coord. Chem. Rev. 380 (2019) 550–571.
[15] Y.Duan Kenry, B. Liu, Adv. Mater. 30 (2018) 1802394.
[16] H. Lin, Z. Lin, K. Zheng, et al., Adv. Opt. Mater. 9 (2021) 2002177.
[17] C. Li, Q. Wang, Adv. Ther. 2 (2019) 1900053.
[18] C. Tang, C. Song, Z. Wei, et al., Sci. China Chem. 63 (2020) 946–956.
[19] R. Yang, K. Lou, P. Wang, et al., Small Methods 5 (2021) e2001066.
[20] W. Zeng, X. Wu, T. Chen, et al., Adv. Funct. Mater. 31 (2021) 2008362.
[21] C. Yan, J. Dai, Y. Yao, et al., Nat. Protoc. 18 (2023) 1316–1336.
[22] J. Chen, C. Ning, Z. Zhou, et al., Prog. Mater. Sci. 99 (2019) 1–26.
[23] Z. Jiang, Z. Jiang, Y. Jiang, et al., Colloids Surf. B 228 (2023) 113438.
[24] Y. Yao, P. Ding, C. Yan, et al., Angew. Chem. Int. Ed. 13 (2023) e202218983.
[25] H.S. Han, K.Y. Choi, Biomedicines 9 (2021) 305.
[26] L. Zhao, X. Zhang, X. Wang, et al., J. Nanobiotech. 19 (2021) 335.
[27] K. Yang, S. Zhao, B. Li, et al., Chem. Rev. 454 (2022) 214330.
[28] L. Wan, Y. Cao, C. Cheng, et al., ACS Appl. Mater. Interfaces 15 (2023) 1784–1797.
[29] A.V.P. Kumar, S.K. Dubey, S. Tiwari, et al., Int. J. Pharm. 606 (2021) 120848.
[30] K. Yang, B. Yu, W. Liu, et al., Chin. Chem. Lett. 34 (2023) 107889.
[31] R. Malekzadeh, T. Mortezazadeh, W.K. Abdulsahib, et al., Environ. Res. 236 (2023) 116526.
[32] W. Cheng, H. Chen, C. Liu, et al., View 1 (2020) 20200055.
[33] B. Aydner, Z. Seferolu, Eur. J. Org. Chem. 2018 (2018) 5921–5934.
[34] V.K. Shukla, G. Chakraborty, A.K. Ray, Dyes Pigm. 215 (2023) 111245.
[35] M. Liu, S. Ma, M. She, et al., Chin. Chem. Lett. 30 (2019) 1815–1824.
[36] C. Ma, T. Zhang, Z. Xie, J. Mater. Chem. A. 9 (2021) 7318–7327.
[37] Y. Zhu, J. Liu, M. Lv, et al., Chin. Chem. Lett. 34 (2023) 109446.
[38] J. Gao, R. Wang, T. Zhu, et al., J. Mater. Chem. A. 8 (2020) 9877–9880.
[39] M. Zhang, G.L. Dai, C.J. Zheng, et al., Org. Electron. 99 (2021) 106312.
[40] N. Balsukuri, N.J. Boruah, P.E. Kesavan, et al., New J. Chem. 42 (2018) 5875–5888.
[41] H. Lu, J. Mack, Y. Yang, et al., Chem. Soc. Rev. 43 (2014) 4778–4823.
[42] T. Baron, V. Maffeis, C. Bucher, et al., Chem. Eur. J. 29 (2023) e202301357.
[43] E.A. Zaballa, A.P. Castañeda, F.G. Garrido, et al., Chem. Eur. J. 26 (2020) 16080–16088.
[44] X.D. Jiang, S. Li, B.L. Guennic, et al., Phys. Chem. Chem. Phys. 18 (2016) 32686–32690.
[45] J. Liu, J. Geng, L.D. Liao, et al., Polym. Chem. 5 (2014) 2854–2862.
[46] N. Chen, H. Kommidi, H. Guo, et al., Mater. Sci. Eng. C 111 (2020) 110762.
[47] G. Feng, G.Q. Zhang, D. Ding, Chem. Soc. Rev. 49 (2020) 8179–8234.
[48] C. Chen, H. Ou, R. Liu, et al., Adv. Mater. 32 (2020) 1806331.
[49] M. Zheng, Q. Yang, C. Lu, et al., Drug Discov. Today. 28 (2023) 103598.
[50] R. Lincoln, A.M. Durantini, L.E. Greene, et al., Photochem. Photobiol. Sci. 16 (2016) 178–184.
[51] X.F. Zhang, X. Yang, J. Phys. Chem. B 117 (2013) 5533–5539.
[52] Y. Su, Q. Hu, D. Zhang, et al., Chem. Eur. J. 28 (2022) e202103571.
[53] H.S. Jung, J.H. Lee, K. Kim, et al., J. Am. Chem. Soc. 139 (2017) 9972–9978.
[54] M.R. Zanotelli, J. Zhang, C.A.R. King, Cell Metab. 33 (2021) 1307–1321.
[55] M.D.A. Paskeh, M. Entezari, S. Mirzaei, et al., J. Hematol. Oncol. 15 (2022) 83.
[56] A.E. Ramírez, R.A.C. Rodríguez, S.Z. Vega, et al., Pharmaceuticals 13 (2020) 156.
[57] P. Dey, A.C. Kimmelman, R.A. DePinho, Cancer Discov. 11 (2021) 1067–1081.
[58] E. Belyaeva, R.K. Kharwar, I.V. Ulasov, et al., Mol. Cell. Biochem. 477 (2022) 593–604.
[59] E. Petrosyan, J. Fares, A. Cordero, et al., Int. J. Cancer 151 (2022) 167–180.
[60] H. Yamamoto, S. Zhang, N. Mizushima, Nat. Rev. Genet. 24 (2023) 382–400.
[61] M. Abate, A. Festa, M. Falco, et al., Semin. Cell Dev. Biol. 98 (2020) 139–153.
[62] Z. Darzynkiewicz, E. Bedner, P. Smolewski, Semin. Hematol. 38 (2001) 179–193.
[63] M.E. Christensen, E.S. Jansen, W. Sanchez, et al., Methods 61 (2013) 138–145.
[64] Z. Luo, X. Xu, T. Sho, et al., Am. J. Physiol. Cell Physiol. 316 (2019) C198–C209.
[65] J.R. Garbow, T.M. Johanns, X. Ge, et al., Front Oncol. 11 (2021) 693146.
[66] W. Zhao, L. Zhang, Y. Zhang, et al., Cell Death Dis. 14 (2023) 11.
[67] L.W. Ren, W. Li, X.J. Zheng, et al., Acta Pharmacol. Sin. 43 (2022) 194–208.
[68] M.R. Kolbe, T. Hohmann, U. Hohmann, et al., Cancers 13 (2021) 1064.
[69] Z. Yao, X. Jiang, H. Yao, et al., Biomater. Res. 26 (2022) 71.
[70] W. Zheng, Q. Chen, H. Liu, et al., Autophagy 19 (2023) 839–857.